LM-06K006
March 9, 2006

# Quaternary InGaAsSb Thermophotovoltaic Diodes

MW Dashiell, JF Beausang, H Ehsani, GJ Nichols, DM Depoy. LR Danielson, P Talamo, KD Rahner, EJ Brown, SR Burger, PM Fourspring, WF Topper, PF Baldasaro, CA Wang, R Huang, M Connors, G Turner, Z Shellenbarger, G Taylor, J Li, R Martinelli, D Donetski, S Anikeev, G Belenky and S Luryi

# Quaternary InGaAsSb Thermophotovoltaic Diodes

M.W. Dashiell, J.F. Beausang, H. Ehsani, G.J. Nichols, D.M. Depoy, L.R. Danielson, P. Talamo, K.D. Rahner, E.J. Brown, S.R. Burger, P.M. Fourspring, W.F. Topper, P.F. Baldasaro,
*Lockheed Martin Corporation, Schenectady, New York 12301-1072*

C.A. Wang, R. Huang, M. Connors, G. Turner,
*MIT Lincoln Laboratory, Lexington Massachusetts 02420-9108*

Z. Shellenbarger, G. Taylor, Jizhong Li, R. Martinelli,
*Sarnoff Corporation, Princeton, New Jersey 08543-5300*

D. Donetski, S. Anikeev, G. Belenky and S. Luryi
*State University of New York, Stony Brook, New York 11794-2350*

**ABSTRACT.**

$In_xGa_{1-x}As_ySb_{1-y}$ thermophotovoltaic (TPV) diodes were grown lattice-matched to GaSb substrates by Metal Organic Vapor Phase Epitaxy (MOVPE) in the bandgap range of $E_G$ = 0.5 to 0.6eV. InGaAsSb TPV diodes, utilizing front-surface spectral control filters, are measured with thermal-to-electric conversion efficiency and power density of $\eta_{TPV}$ =19.7% and $PD$ =0.58 W/cm$^2$ respectively for a radiator temperature of $T_{radiator}$ = 950°C, diode temperature of $T_{diode}$ = 27°C, and diode bandgap of $E_G$ = 0.53eV. Practical limits to TPV energy conversion efficiency are established using measured recombination coefficients and optical properties of front surface spectral control filters, which for 0.53eV InGaAsSb TPV energy conversion is $\eta_{TPV}$ =28% and $PD$ =0.85W/cm$^2$ at the above operating temperatures. The most severe performance limits are imposed by (i) diode open-circuit voltage ($V_{OC}$) limits due to intrinsic Auger recombination and (ii) parasitic photon absorption in the inactive regions of the module. Experimentally, the diode $V_{OC}$ is 15% below the practical limit imposed by intrinsic Auger recombination processes. Analysis of InGaAsSb diode electrical performance vs. diode architecture indicate that the $V_{OC}$ and thus efficiency is limited by extrinsic recombination processes such as through bulk defects.

## I. INTRODUCTION

Low bandgap (low $E_G$) TPV converters have attracted interest in the field of direct energy conversion due to the potential for efficient electric generation [1-3]. The best reported TPV efficiencies, measured at $T_{radiator}$=950 °C and $T_{diode}$=27 °C, are $\eta_{TPV}$=22% for $E_G$=0.6eV InGaAs/InP [4] and $\eta_{TPV}$=19.7% for $E_G$=0.53eV InGaAsSb/GaSb diodes [3]. Both systems utilized spectral control filters mounted on the front surface of the diode in order to recuperate below bandgap radiation [5-6]. Quaternary InGaAsSb alloys were investigated because they can be grown lattice-matched to GaSb substrates for bandgaps as low as 0.5eV [7-11]; to date however, the material underperforms compared to ternary InGaAs TPV diodes. This article summarizes the theory used to predict the practical TPV thermal-to-electric energy conversion efficiency for heat transferred radiatively from a hot side radiator to cold side diode module. Our analysis uses measured minority carrier recombination coefficients to determine the intrinsic limits to 0.53eV InGaAsSb TPV diode power conversion efficiency and assesses the electronic material quality and architecture required to approach these bounds. Figure 1 shows the architecture of a typical InGaAsSb n/p junction diode investigated during this work. A TPV module refers to the combination of front surface spectral control filter and the TPV diode or an array of diodes.

## II. THERMOPHOTOVOLTAIC EFFICIENCY ($\eta_{TPV}$)

TPV thermal-to-electric power conversion efficiency $\eta_{TPV}$ is defined as the electrical power output from the TPV module divided by the total thermal power absorbed in the module. The thermal power transferred from the hot ($T_{Radiator}$) radiator to the cold module ($T_{Diode}$) is due to radiative heat transfer across a vacuum gap. The maximum electrical power from the TPV diode is the product of the open circuit voltage ($V_{OC}$), the short circuit current ($I_{SC}$), and the fill factor ($FF$) [12]. Because photons having energies ($E < E_G$) cannot be converted into electricity it is convenient to evaluate the overall efficiency as the product of the diode efficiency $\eta_{Diode}$ and the spectral efficiency $\eta_{Spectral}$ [1,3]. The term $\eta_{Diode}$ quantifies the power conversion efficiency for above bandgap ( $E > E_G$ ) thermal radiation absorbed in the diode's active n/p junction area,. The term $\eta_{Spectral}$ quantifies the ratio of above bandgap radiation absorbed in the active area divided by the total thermal radiation absorbed in the module. The breakdown of these efficiency parameters are given in Table A1 of the Appendix. The overall expression for TPV thermal-to-electric power conversion efficiency $\eta_{TPV}$ is:

$$\eta_{TPV} = \eta_{Spectral} \times \eta_{Diode} = \frac{V_{OC} \times I_{SC} \times FF}{A_{Total} \int_0^{\infty} \varepsilon_{eff}^{Cavity} \frac{2\pi E^3}{h^3 c^2 (e^{E/kT_{Radiator}} - 1)} dE} \quad (1)$$

Where $E$, $h$, $k$, $c$ and $T_{radiator}$ are photon energy, Planck's constant, Boltzmann's constant, the speed of light and the radiator (hot side) temperature. The effective cavity emissivity $\varepsilon_{eff}^{cavity}$ modifies Planck's spectral distribution to account for non-blackbody emission and absorption in the optical cavity.

While thermodynamic analysis [1,13,14] can provide a theoretical maximum to TPV conversion efficiency, non-radiative electronic recombination in the diode and parasitic absorption in the module must be quantified both with experimental material data and mathematical models. This article uses established semiconductor theory and empirically determined values of InGaAsSb material coefficients [15-17] and the optical properties of front surface spectral control filters [5-6] to determine a practical limit to TPV conversion efficiency applied to the 0.53eV InGaAsSb TPV material system.

### IIIa SPECTRAL CONTROL MODELING ASSUMPTIONS

Due to optical absorption losses, particularly for photon energies below the diode bandgap, the best reported spectral efficiencies are $\eta_{Spectral} \sim 80\%$ for the 0.53eV bandgap and $T_{radiator}$=950°C [5,6]. For simplicity, spectral performance calculations in this analysis assume a step function reflection profile where the filter reflects 97% of below bandgap photons, reflects 15% of above bandgap photons and has a ~2% parasitic absorbance of above bandgap photons in the filter at all incident photon angles. These values project a practical limit to 0.53eV TPV spectral efficiency based on the optical properties and design optimization studies of front surface filters. The practical limit to spectral efficiency using the approximations detailed in Table AI of the appendix is determined to be $\eta_{Spectral} = 87\%$.

### IIIb TPV DIODE RECOMBINATION MODELS

The net radiative recombination rate per unit volume, calculated from the Shockley van Roosbroek (SvR) detailed-balance method [18], must be corrected because some of the light emitted during radiative recombination will be reabsorbed (recycled) in the active region of the TPV diode. The net radiative recombination rate used in the simulations, is given by equation (2)

$$R_{Rad} = \frac{B}{\varphi}( np - n_i^2 ) \quad (2)$$

Where $Bn_i^2$ is the net thermal equilibrium rate of radiative recombination per unit volume, calculated via the SvR relation. The photon recycling factor ( $\varphi$ ) [19,20] is the inverse ratio of the sum of the photon flux exiting the diode's front and back surfaces to the total number of radiative recombination events occurring within the diode volume (Table AII). The quantities $n$ and $p$ in equation (2) are the electron and hole carrier densities under illumination and $n_i$ is the intrinsic carrier density.

Non-radiative recombination is a parasitic loss which includes Auger recombination and recombination via bulk defect and interface states that lie near the center of $E_G$ (Shockley Read Hall - SRH- recombination). The net Auger recombination rate is given by equation (3)

$$R_{Aug} = ( C_n n + C_p p )( np - n_i^2 ) \quad (3)$$

and the bulk SRH and surface/interface recombination rates due to electronic defect states near the center of the bandgap are modeled by equations (4) and (5) respectively

$$R_{SRH} = \frac{( np - n_i^2 )}{\tau_n( p + n_i ) + \tau_p( n + n_i )} \quad (4)$$

$$R_{SRV} = \frac{S_n S_p( np - n_i^2 )}{S_n( p + n_i ) + S_p( n + n_i )} \quad (5)$$

The recombination coefficients $\tau_{n,p}$ (SRH lifetimes), $S_{n,p}$ (effective surface recombination velocities), and $C_{n,p}$ (Auger coefficients) were parametrically varied in the simulations about values reported in minority carrier lifetime studies of InGaAsSb materials [15-17].

### IVa. INTRINSIC LIMITATIONS TO TPV DIODE OPEN CIRCUIT VOLTAGE: $V_{OC}$

The open-circuit voltage, $V_{OC}$, is a thermodynamically limited quantity since it is a measure of the maximum electrical work that could be performed per unit electronic charge. The ideal diode equation expresses $V_{OC}$ as a function of $T_{Diode}$, the light generated current $I_{Light}$ , and the dark current $I_0$ . The constants $k$ and $q$ are Boltzmann's constant and the electron charge respectively and $n$ is the ideality factor.

$$V_{OC} \approx \frac{nkT_{diode}}{q} ln\left( \frac{I_{light} - I_o}{I_o} \right) \quad (6) .$$

The diode carrier generation/recombination rates which maintain thermal equilibrium with the cold side temperature $T_{Diode}$ determine the diode's dark current ( $I_0$ ) - also known as reverse saturation

current [1,12-14]. Bounding the TPV diode active region with a back surface reflector (BSR) rather than an absorbing substrate or back contact, minimizes the radiative component of $I_0$ because the BSR reduces the number of available photon modes that contribute to the overall equilibrium generation/recombination rates [1] and sets the thermodynamic maximum to $V_{OC}$. In addition the ideal BSR will increase the optical path length by a factor of two, enabling a reduction of the volumetric non-radiative recombination processes which are unavoidable in real diodes. In concept, $V_{OC}$ limitations due to additional extrinsic generation/recombination processes such as bulk SRH defect recombination might be eliminated, however, Auger recombination is a fundamental non-radiative process which can be minimized, but not eliminated, by reducing background carrier densities and absorber thickness. Attempts to reduce Auger recombination limitations to $V_{OC}$ by reducing background doping will ultimately result in the diode going into high injection. The high injection Auger recombination rate determines the lowest possible non-radiative recombination rate under illuminated conditions and thus sets the intrinsic material limit to $I_0$ and $V_{OC}$ [21].

Using the narrow base approximations from reference [21], an estimate for the values of the extrinsic coefficients $S_{n,p}$ and $\tau_{n,p}$ required to approach the intrinsic Auger limited open circuit voltage can be made. The authors of reference [21] determined the $V_{OC}$ limits as a function of light generated current density $J_{Light}$ for absorbing region of background doping $N_B$ and thickness $W$ for each of the recombination processes given in eqns (2-5). In a "defect-free" material the optimum background doping ($N_B$ ) and the intrinsic Auger limited $V_{OC}$ is reached when the illuminated diode enters the high-injection regime. For a p-type absorbing region the bulk electronic material quality is deemed sufficient to approach this intrinsic limit only when the bulk SRH minority carrier lifetime is greater than the quantity given in equation (7).

$$\tau_p^{high-injection} >> \left[ q^2 W^2 \Big/ J_{Light}^{\,2} (C_P + C_n) \right]^{1/3} \qquad (7)$$

Reference [15] reports values of the Auger coefficient of $C \approx 2\times10^{-28}\text{cm}^6/\text{s}$ in 0.53eV InGaAsSb. Thus for light generated currents of $J_{Light} \approx 3\text{A/cm}^2$, the bulk SRH lifetime must be greater than $\tau_{n,p} >> 1\mu\text{s}$ in both n-type and p-type InGaAsSb in order to approach the intrinsic Auger limited $V_{OC}$ . Using the same approach the front and back surface/interface recombination velocities need to be $S_{n,p} \leq 100\text{cm/s}$ and the photon recycling factor must be $\varphi >> 5$ to approach the intrinsic Auger limited $V_{OC}$. The last requirement means the InGaAsSb TPV diode requires a back surface reflector in order

for the radiative recombination rate to be small compared to the intrinsic Auger recombination rate (see Table A2).

Measured minority carrier lifetimes in **p-type** double heterostructure (DH) InGaAsSb samples give bulk values of $\tau_p$~1μs and $S_p \approx$ 700-2000cm/s at the interfaces [15-17]. However unlike p-type InGaAsSb, **n-type** InGaAsSb exhibits a strong excitation dependence of the carrier lifetime which shows the material is dominated by electrically active SRH type defects. The excitation dependence makes a precise measurement/model for the SRH lifetime at the relevant light injection levels in n-type InGaAsSb (Te-doped) difficult, however the preliminary measurements set bounds of $\tau_n \geq 0.1\mu s$ in n-type InGaAsSb and $S_n \leq 2000$cm/s at the n-type interfaces. Comparison of measured n-type and p-type InGaAsSb recombination parameters with those values required to approach the intrinsic Auger limit indicate that the electronic material quality of 0.53eV InGaAsSb is not sufficient to approach the intrinsic Auger limited $V_{OC}$ at these light generated currents.

### IVb. INTRINSIC LIMITATIONS TO TPV DIODE SHORT CIRCUIT CURRENT AND FILL FACTOR

Unlike $V_{OC}$, there are no thermodynamic restrictions to the efficiency in which above bandgap photons can be converted to photogenerated electrons. The primary limitations to $I_{light} \approx I_{SC}$ are due to parasitic absorption and reflections of above bandgap photons in the spectral control filter and other inactive regions of the TPV module (see table A1). Experimental data for 0.53eV InGaAsSb diode indicate that the short circuit current, $I_{SC}$, is not limited by minority carrier recombination in the active region because the minority carrier diffusion lengths are greater than the diode thickness (narrow base) and the effective surface recombination velocities are $S_{n,p}<10^4$cm/s. Theoretically the fill factor (*FF*) also depends on $I_0$, however unlike $V_{OC}$ the *FF* becomes practically limited by series resistances external to the diode active region. Experiments and calculations show that 2mΩ·cm$^2$ is the practical limit to series resistance setting a fill factor limit of FF=0.74 for $J_{SC}$=3A/cm$^2$.

## V. NUMERICAL SIMULATIONS OF 0.53eV InGaAsSb TPV EFFICIENCY AND OUTPUT POWER

Conversion of above bandgap thermal radiation into electric power was calculated using PC-1D, a numerical photovoltaic simulator which solves the carrier transport, Poisson, and carrier continuity equations for electrons and holes. Solutions were cross-checked using the analytic expressions discussed in this article and in [12,21]. Non-equilibrium electron-hole generation rates in

the diode were determined from the absorbed thermal radiation spectrum transmitted through the front surface spectral control filter into the diode.

Figure 2a and 2b show the intrinsic efficiency and power density limits (solid symbols) as a function of the Auger coefficients $C_{n,p}$ for 0.53eV TPV diode module having spectral control properties given in Table AI, a back surface reflector, negligible defect recombination, and operating at the onset to high level injection . The measured Auger coefficient of $C_p=2\times10^{-28}$ $cm^6/s$ from [15] determines the best estimate to the practical/intrinsic limit for 0.53eV InGaAsSb TPV. Figure 2 shows that by raising $T_{diode}$ from 27°C to 100°C the practical efficiency limit drops from $\eta_{TPV}$=28% to $\eta_{TPV}$=18%, due to the strong temperature dependence of the intrinsic carrier density. The open-symbols of figure 2a and 2b show the efficiency and power density limits for 0.53eV TPV diodes having non-negligible extrinsic recombination losses ($\tau_{n,p}$=1μs and $S_{n,p}$=500cm/s) illustrating the stringent material requirements necessary to approach the intrinsic limit.

Figure 3 shows the simulated diode $V_{OC}$ as a function of p-type doping ($N_A$) for the general architecture shown in Fig 1. The uppermost curve in Fig. 3 corresponds to an architecture having an ideal back surface reflector and two-pass optical path length ($\varphi$=40) and negligible defect recombination ($\tau_{n,p}$=10μs, $S_{n,p}$=10cm/s). The high-level injection ($N_A \leq 5\times10^{16}$ $cm^{-3}$) Auger recombination rate sets the intrinsic limit to $V_{OC}$ of 370 mV for the assumed operating temperatures. The second uppermost curve simulates the same InGaAsSb material quality ($\tau_{n,p}$=10μs, $S_{n,p}$=10cm/s), but having an absorbing substrate and single-pass optical path length (photon recycling factor $\varphi$=4) where the decrease in maximum achievable $V_{OC}$ to 340mV is due to the increased radiative dark current and increased thickness to account for the single-pass optical path length. The remaining curves show the degradation in $V_{OC}$ for increasing extrinsic interface recombination losses ($S_n=S_p=S$), demonstrating that the high injection regime is no longer optimal for diodes limited by defect recombination and illustrating the severe $V_{OC}$ degradation. Similar trends were observed when the TPV diode becomes bulk SRH defect limited. The numerical simulations give good agreement with the closed form analysis of Section IV stating that the extrinsic parameters must be $\tau_{n,p} >> 1\mu s$ and $S_{n,p} \leq 100cm/s$ in order to approach the intrinsic Auger limit.

## VI. MEASURED 0.53eV InGaAsSb TPV DIODE ELECTRICAL/OPTICAL CHARACTERISTICS

Both n/p (thin-emitter) and p/n (thick-emitter) 0.53eV InGaAsSb double heterostructure TPV diodes were fabricated using standard photolithography and metal evaporation [10,23] having an area of 0.5cm$^2$. To prevent minority carriers from diffusing to a free semiconductor surface, the diode is passivated with either GaSb ($E_G \approx 0.73$eV) or AlGaAsSb ($E_G \approx 1.0$eV) window layers [8-10] as shown in Fig 1. Both GaSb and AlGaAsSb back surface fields (BSF) were investigated to confine minority carriers at the rear of the active diode. A doped GaSb contact layer was grown subsequent to the window layer to enable ohmic contact formation for the metal contact grid. The influence of parasitic series ($r_{series}$ <0.005 Ω·cm$^2$) and shunt resistances ($r_{shunt}$ >50 Ω·cm$^2$) were negligible near the operating conditions.

## VIa. INTERNAL QUANTUM EFFICIENCY MEASUREMENTS OF 0.53eV InGaAsSb TPV DIODES.

Figure 4 shows the measured ($T_{Diode}$= 27°C) internal quantum efficiency (IQE) responses for n/p and p/n 0.53eV InGaAsSb TPV diodes. The IQE response is the same for both n/p and p/n architectures having thin (<200nm) GaSb window/contact layers (refer to figure legend). The high IQE between 1600nm and 2250nm indicate a diffusion length for electrons (holes) in excess of the p-type absorber thickness (thin n-type thickness) which is consistent with simulations and references [7,10]. The measured IQE degrades at wavelengths below 1600nm, corresponding to the GaSb absorption cutoff wavelength [24]. Simulations indicate that a significant fraction of minority carriers generated in the GaSb contact layer may recombine at the unpassivated GaSb free surface ($S_{surface}\approx 10^5$cm/s) while the remainder may diffuse into the active InGaAsSb region and be collected as photocurrent. Experimental short wavelength IQE response degraded upon increasing GaSb contact thicknesses which supports this conclusion.

The third data set in Fig. 4 shows the measured IQE response for an n/p architecture having a thick GaSb contact layer (>400nm) and AlGaAsSb passivating window layer. Severe short wavelength IQE degradation is observed in this third curve for two reasons. First, the IQE experiences additional degradation at short wavelengths because the GaSb contact layer is more than twice as thick as for the previous two curves. Secondly, the high $E_G$ of the AlGaAsSb layer relative to both the GaSb contact layer and the InGaAsSb active region causes it to act as a diffusion barrier to minority carriers generated in the GaSb, which was confirmed by comparing measured responses from the two window materials having equivalent GaSb contact thicknesses. The high $E_G$ AlGaAsSb

window between InGaAsSb active region and GaSb prevents nearly all minority carriers generated in the GaSb contact from diffusing into the active InGaAsSb, which degrades the short wavelength IQE response compared to using GaSb windows. The generic band diagrams in the vicinity of the emitter for n/p diodes are shown in the inset of Figure 4 which illustrate these two mechanisms. Note that the effect of this degradation on TPV efficiency and short circuit current is small (< 5% relative) due to the limited radiation spectrum below 1600nm expected from a 950°C radiator.

### VIb. CURRENT VOLTAGE MEASUREMENTS OF N/P AND P/N 0.53eV InGaAsSb TPV DIODES HAVING GaSb OR AlGaAsSb DOUBLE-HETEROJUNCTION CONFINEMENT

Figure 5 shows the open-circuit-voltage vs. short-circuit-current density ($V_{oc}$-$J_{SC}$) relation for six 0.53eV InGaAsSb TPV n/p and p/n diode architectures. The measured $V_{OC}$ varies logarithmically with $J_{SC}$, as expected from the ideal diode model and near unity ideality ($1.0 < n < 1.1$) was observed for all architectures for $J_{SC}$ values greater than 0.1A/cm$^2$. The lowest measured dark currents were $J_o$=1.5×10$^{-5}$ A·cm$^{-2}$ for p/n diodes having AlGaAsSb windows and n/p diodes having either GaSb or AlGaAsSb windows. For $J_{SC}$ > 0.1A/cm$^2$, well above our expected operating currents, the current voltage characteristics for both n/p and p/n architectures were insensitive to whether the BSF interface was GaSb/InGaAsSb or AlGaAsSb/InGaAsSb. However p/n diodes with GaSb window layers have larger room temperature dark currents of $J_o$=2.5×10$^{-5}$ A/cm$^2$ which is attributed to greater than twofold increase in the front surface recombination velocity. Measured surface recombination velocities at p-type AlGaAsSb/InGaAsSb interfaces yielded average measured values of $S_p$~700cm/s, whereas the p-type InGaAsSb/GaSb interfaces yield an average value of $S_p$~2000cm/s [15-17]. The dependence of experimental $J_0$ for diodes having p-GaSb and p-AlGaAsSb minority confinement layers provide further insight on the results of reference [15-17]. P-type AlGaAsSb front surface windows reduce $J_0$ in p/n diodes compared to p-type GaSb windows, however, both p-type AlGaAsSb and GaSb BSFs yield nearly equivalent $J_0$ for n/p diodes. The asymmetry indicates that p-type AlGaAsSb passivation layer (due to its higher $E_G$) suppresses minority carrier diffusion to the free surface of the GaSb contact layer, however its effect (if any) on the number of defect states at the interface does not influence $J_0$. Because the AlGaAsSb causes a degradation in the IQE, an n/p design using thin GaSb window may be optimum for both short wavelength photoresponse and high $V_{OC}$.

Two simulated $V_{OC}$-$J_{SC}$ curves are also shown in Figure 5. The first simulation (solid line) gives a reasonable agreement (but slightly better) to the measured data by assuming recombination coefficients of $C_{n,p}=2\times10^{-28}cm^6/s$, $\tau_{SRH}$ = 1 μs, $S_{n,p}$=1000cm/s and an absorbing back surface ($\phi$=4). The second simulation (dotted line) shows the practical limit for a BSR diode architecture ($\phi$=40) having negligible extrinsic recombination processes, illustrating the potential gains in $V_{OC}$ with reduction in the extrinsic recombination losses.

### VIc. INFLUENCE OF DOPING AND ARCHITECTURE ON 0.53eV InGaAsSb TPV DIODE PERFORMANCE

A summary of the measured $V_{OC}$ (at $J_{Light} = J_{SC}$ ~2.5A/cm$^2$) for various n-type and p-type doping levels, and minority carrier confinement layer compositions is shown in Table I. Along with the carrier confinement layers, are the corresponding estimates for the interface recombination velocities $S_{n,p}$ from references [15-17]. The open circuit voltage was normalized to the bandgap ($V_{OC}/E_G$) to account for slight variations in alloy composition observed during the many growth runs performed. Included also in Table I is the 0.53eV InGaAsSb hybrid back surface reflector device reported in [22] which will have greater photon recycling compared to that of a thick absorbing GaSb substrate. All diodes listed in Table I had measured fill factors of FF=0.7±0.02 and peak IQEs near ~100%.

The only significant change in $V_{OC}/E_G$ was observed for p/n architectures when the effective front surface recombination velocity was increased from ~700cm/s to ~2000cm/s when using the p-type GaSb window rather than AlGaAsSb. Table I shows that $V_{OC}/E_G$ remains unchanged for either n-type and p-type doping ranging from mid $10^{16}cm^{-3}$ to low $10^{18}cm^{-3}$. In addition, $V_{OC}/E_G$ also did not increase beyond a maximum value of $V_{OC}/E_G$ = 0.6 when the p-type AlGaAsSb/InGaAsSb SRV was reduced to $S_p$~30cm/s by optimizing the interfacial growth conditions [17]. Finally, $V_{OC}$ did not increase upon thinning the GaSb substrate and incorporating a BSR, although a small increase in long wavelength quantum efficiency was observed due to the increase in the effective optical path length with the BSR [22].

The observed independence of the measured $V_{OC}/E_G$ on InGaAsSb doping levels ranging from mid $10^{16}cm^{-3}$ to low $10^{18}cm^{-3}$ (changing low injection Auger lifetime), optical boundary conditions (changing photon recycling), and upon reducing the surface recombination velocity to values near $S_p$ ~ 30cm/s, as well as the absolute value of the experimental $V_{OC}$ follows that behavior predicted for a

diode whose $V_{OC}$ is limited by extrinsic material recombination processes. The experimental diode measurements are in agreement with the discussion of Section IV, where the measured values of the extrinsic recombination coefficients ($\tau_{n,p}$ and $S_n$) do not meet the requirements to obtain the practical limit to $V_{OC}$. Based upon this we conclude that extrinsic defect recombination mechanisms limit InGaAsSb diode output voltage and efficiency in contrast to the conclusions of reference [7]

**Table I Summary of 0.53eV InGaAsSb architectures and measured open circuit voltages. *The reported interface recombination velocities are an average value of front and back interfaces in the double heterostructure lifetime structures of refs. [15-17].**

| InGaAsSb Architecture | InGaAsSb n-type doping | n-type confinement | $S_n$ (cm/s) * | InGaAsSb p-type doping | p-type confinement | $S_p$ (cm/s) * | BSR | $V_{OC}/E_{gap}$ @ 2.5Acm$^{-2}$ |
|---|---|---|---|---|---|---|---|---|
| n/p | $1\times10^{18}$cm$^{-3}$ | GaSb | < *2000* | ***5×10$^{16}$cm$^{-3}$*** | AlGaAsSb | ~700 | No | 0.60 ± 0.015 |
| n/p | $1\times10^{18}$cm$^{-3}$ | AlGaAsSb | < *2000* | ***2×10$^{17}$cm$^{-3}$*** | AlGaAsSb | ~700 | No | 0.59 ± 0.015 |
| n/p | $1\times10^{18}$cm$^{-3}$ | GaSb | < *2000* | ***2×10$^{17}$cm$^{-3}$*** | GaSb | ~2000 | No | 0.59 ± 0.015 |
| p/n | $1\times10^{18}$cm$^{-3}$ | GaSb | < *2000* | ***2×10$^{17}$cm$^{-3}$*** | AlGaAsSb | ~700 | No | 0.60 ± 0.015 |
| p/n | $1\times10^{18}$cm$^{-3}$ | GaSb | < *2000* | ***2×10$^{17}$cm$^{-3}$*** | AlGaAsSb | ~700 | Yes | 0.60 ± 0.015 |
| p/n | $1\times10^{18}$cm$^{-3}$ | GaSb | < *2000* | ***2×10$^{17}$cm$^{-3}$*** | AlGaAsSb | ~30 | No | 0.60 ± 0.015 |
| p/n | $1\times10^{18}$cm$^{-3}$ | GaSb | < *2000* | ***2×10$^{17}$cm$^{-3}$*** | GaSb | ~2000 | No | 0.55 ± 0.015 |
| p/n | $1\times10^{18}$cm$^{-3}$ | GaSb | < *2000* | ***4×10$^{17}$cm$^{-3}$*** | AlGaAsSb | ~700 | No | 0.58 ± 0.015 |
| p/n | $1\times10^{18}$cm$^{-3}$ | GaSb | < *2000* | ***1×10$^{18}$cm$^{-3}$*** | AlGaAsSb | ~700 | No | 0.59 ± 0.015 |
| p/n | ***1×10$^{17}$cm$^{-3}$*** | GaSb | < *2000* | $2\times10^{17}$cm$^{-3}$ | AlGaAsSb | ~700 | No | 0.58 ± 0.015 |
| p/n | ***2×10$^{17}$cm$^{-3}$*** | GaSb | < *2000* | $2\times10^{17}$cm$^{-3}$ | AlGaAsSb | ~700 | No | 0.58 ± 0.015 |
| p/n | ***3×10$^{17}$cm$^{-3}$*** | GaSb | < *2000* | $2\times10^{17}$cm$^{-3}$ | AlGaAsSb | ~700 | No | 0.59 ± 0.015 |
| p/n | ***3×10$^{18}$cm$^{-3}$*** | GaSb | < *2000* | $2\times10^{17}$cm$^{-3}$ | AlGaAsSb | ~700 | No | 0.59 ± 0.015 |

## VII. 0.5-0.6eV InGaAsSb TPV DIODES LATTICE MATCHED TO GaSb

Bandgap flexibility, is an important consideration when choosing a TPV diode material because the optimal diode bandgap depends on both $T_{Diode}$ and $T_{radiator}$. Figure 6 shows the experimental dark current $J_0$ vs. $E_G$ for p/n InGaAsSb TPV diodes grown on GaSb substrates (circles). The ideality factor for all InGaAsSb bandgaps was measured to be ($1.0 < n < 1.05$) and all fill factors were measured to be FF=0.70 ±0.02. Measured InGaAsSb dark currents vary proportionally to $J_0 \alpha \exp(-E_G/kT_{Diode})$ indicating that (i) square of the intrinsic carrier density

dominates the InGaAsSb dark current characteristics and thus (ii) the electronic material quality is not significantly different over this bandgap range despite the material approaching the miscibility gap [9]. We note that the 0.6eV InGaAsSb diode probably has a slightly larger front SRV compared to lower bandgaps due to the smaller window band offset [17]. As a qualitative materials comparison experimental $J_0$ of 0.6eV InGaAs/InP diodes, representative of 22% efficient diodes [4], is shown in Fig. 6 (triangle). The dark current for 0.6eV InGaAs/InP lies well below that of the InGaAsSb/GaSb empirical data and fit, suggesting that the ternary InGaAs possesses superior photovoltaic material properties over the quaternary InGaAsSb alloy. High densities of anti-site defects in antimonide based semiconductors are responsible for the observed high p-type background concentration and donor-anti-site species have been reported to be also be associated with deep levels [27]. There is not however sufficient published defect spectroscopy on low $E_G$ InGaAsSb opto-electronic devices to actually correlate anti-site defects with diode dark current. Further work determining the defect structure in p-type and n-type InGaAsSb and the Shockley-Read-Hall lifetime in n-type tellurium doped InGaAsSb would provide additional data. Comparison of best SRH lifetimes ($\tau_p$~1μs) measured in InGaAsSb [15] with values of $\tau_p$~5-14μs reported for GaAs photovoltaic material [25,26] are further evidence of significant bulk defect activity in the InGaAsSb alloy system.

## VIII. MEASUREMENTS OF 0.53eV InGaAsSb THERMAL-TO-ELECTRIC TPV CONVERSION EFFICIENCY ($\eta_{TPV}$)

The performance of 0.53eV InGaAsSb TPV diode modules (1cm$^2$ and 4cm$^2$ areas) were measured in a prototypic vacuum test cavity, described in reference [3,4,28]. The photonic cavity is prototypical of a flat-plate TPV generator design, where the radiator is a large flat silicon carbide surface. The TPV module was fixed to the top of a copper pedestal to facilitate heat absorption measurements. Thermal-to-electric efficiency in this test was measured as the ratio of peak module electric power to total module heat absorption rate. These parameters were measured simultaneously to assure validity of the final efficiency value. A front surface filter, with spectral efficiency calculated from reflection data to be $\eta_{Spectral}$≈79%, is joined to the modules with optical epoxy. Table II gives the measured efficiency and electrical parameters of the 0.53eV InGaAsSb TPV module. As predicted, $V_{OC}$, $PD$, and $\eta_{TPV}$ decrease with increasing temperature $T_{Diode}$. At 30°C the average 0.53eV InGaAsSb TPV efficiency is only ~70% of the practical limit to efficiency based on the intrinsic Auger recombination processes. The largest fractional difference in the experimental performance vs. the intrinsic limits is due to the diode

open circuit voltage, ($V_{OC}$ = 306mV vs. 370mV), with the remainder attributed to spectral performance ($\eta_{spectral}$ = 79% vs. 87%) and module fill factor (FF = 67% vs. 74%) and the percent active area ($A_{active}$ = 84% vs. 90%). Based on the previous discussion, extrinsic recombination processes limit the InGaAsSb TPV diode $V_{OC}$, making this the most significant barrier to reaching the practical efficiency limits .

**Table II. Measured thermal-to-electric efficiencies for 0.53eV InGaAsSb TPV diode modules.**

| TPV Diode Parameter | $T_{diode} \approx 30°C$ | $T_{diode} \approx 50°C$ | $T_{diode} \approx 70°C$ |
|---|---|---|---|
| Radiator Temperature | 950°C | 950°C | 950°C |
| Average $V_{OC}$ per diode (volts) | 0.306 | 0.273 | 0.247 |
| $J_{SC}$ (Amps/cm$^2$) | 2.9 | 3 | 3 |
| Module Fill Factor (%) | 67 | 63 | 60 |
| PD Power Density (W/cm$^2$) | 0.58 | 0.52 | 0.45 |
| $\eta_{TPV}$ Thermal to Electric Efficiency (%) | 19.7 | 16.9 | 14.6 |

## IX. Conclusions

A practical limit of $\eta_{TPV}$=28% and $PD$ =0.85W/cm$^2$ for 0.53eV InGaAsSb TPV diodes operating at $T_{radiator}$ =950°C and $T_{diode}$ =27°C is established. The most severe bound to low bandgap TPV diode performance will be set the intrinsic Auger limit to open circuit voltage, which for 0.53eV InGaAsSb will be $V_{OC}^{Max}$ = 370mV. Measured InGaAsSb TPV efficiency and power density indicate that InGaAsSb TPV diodes operate well below the intrinsic performance limits, primarily because the diode $V_{OC}$ is dominated by extrinsic recombination processes such as through bulk defect levels. The semi-empirical method used in this article can be applied to other TPV systems and operating conditions, where Auger recombination becomes particularly important if the diode operating temperature increase and/or diode bandgap decreases, since the Auger recombination coefficients and intrinsic carrier density increase exponentially as $E_G$ is reduced and $T_{diode}$ is increased. Using the ranges of Auger coefficients vs. $E_G$ reported in ref. [7], our semi-empirical analysis determine that intrinsic Auger recombination limits to open circuit voltage and efficiency become more severe as the bandgap is reduced below $E_G$ < 0.5eV for the temperatures considered in this work. Below $E_G$ < 0.3eV, the practical limit to TPV efficiency becomes restricted to values below $\eta_{TPV}$ =10% for the above operating conditions and the spectral assumptions of Table AI.

# Appendix

**Table AI Spectral assumptions made for $E_G$=0.53eV TPV Predictions**

| | |
|---|---|
| Radiator temperature | $T_{rad}$=950°C |
| Module area | $A_1$ = 1cm$^2$ Total cell area, $A_2$ = 0.9cm$^2$ Active cell area |
| Radiator emissivity | $\varepsilon_{rad1}$ = 0.9 above band gap > $E_G$, $\varepsilon_{rad2}$ = 0.9 below band gap < $E_G$ |
| TPV diode module reflectivity | $R_1$= 0.97 < $E_G$, active area, $R_2$= 0.15 > $E_G$, active area<br>$R_3$= 0.97 < $E_G$,, inactive area, $R_4$= 0.97 > $E_G$,, inactive area |
| Parasitic absorbance | $f_{parasitic}$=0.02 (fraction of above bandgap radiation absorbed in filter) |
| Area weighted module emissivity at cold side | $\varepsilon_{mod\,1} = \frac{A_2}{A_1}(1-R_2)+(1-\frac{A_2}{A_1})(1-R_4)$ : > $E_G$,<br>$\varepsilon_{mod\,2} = \frac{A_2}{A_1}(1-R_1)+(1-\frac{A_2}{A_1})(1-R_3)$ : < $E_G$, |
| Effective emissivity of radiator / module optical cavity | $\varepsilon_{eff\,1}^{cavity} = \left(\frac{1}{\varepsilon_{rad1}}+\frac{1}{\varepsilon_{mod1}}-1\right)^{-1}$ : > $E_G$<br>$\varepsilon_{eff\,2}^{cavity} = \left(\frac{1}{\varepsilon_{rad2}}+\frac{1}{\varepsilon_{mod2}}-1\right)^{-1}$ : < $E_G$ |
| Total heat absorbed in active region that can be converted to electricity | $P_1 = A_2\int_{E_G}^{\infty}\frac{\varepsilon_{eff\,1}^{cavity}(1-R_2)}{\varepsilon_{mod1}}\frac{2\pi E^3 dE}{h^3c^2(e^{E/kT_{Rad}}-1)}(1-f_{parasitic})$ |
| Total heat absorbed in the cold side module | $P_2 = A_1\int_{Eg}^{\infty}\varepsilon_{eff\,1}^{cavity}\frac{2\pi E^3 dE}{h^3c^2(e^{E/kT_{Rad}}-1)} + A_1\int_0^{E_G}\varepsilon_{eff\,2}^{cavity}\frac{2\pi E^3 dE}{h^3c^2(e^{E/kT_{Rad}}-1)}$ |
| Spectral efficiency | $\eta_{spectral}(E_G = 0.53eV) = \frac{P_1}{P_2} = 87\%$ |
| TPV efficiency | $\eta_{TPV} = \frac{V_{OC}\times I_{SC}\times FF}{P_1}\times\eta_{Spectral} = \eta_{Diodel}\times\eta_{Spectral}$ |

## Table AII 0.53eV InGaAsSb diode parameters used in simulations

| | |
|---|---|
| $T_{Diode}$ and $E_G$ | $T_{300K}$ = 300K / $E_G$(300K) = 0.53eV |
| Density of states | $N_C = 1.5\times10^{17}cm^{-3}$, $N_V = 7\times10^{18}cm^{-3}$ [24] |
| Intrinsic electron density | $n_i^2 = N_C N_V \, exp(-\frac{E_G}{kT_{300K}}) = 4.5\times10^{13}cm^{-3}$ |
| Refractive index | n=3.45 |
| Absorption coefficient | $\alpha(E) = A_o(E - E_G)^{0.5} \; where \; A_o = 2.6\mu m^{-1}eV^{-0.5}$ |
| Radiative recombination coefficient [18] | $B = \frac{1}{n_i^2}\int_{\theta=0}^{\theta=\pi}\int_{\phi=0}^{\phi=2\pi}\int_{E=0}^{E=\infty} n^2\alpha(E)\frac{\partial\Gamma(E)}{\partial E\partial\phi\partial\theta}\sin\theta dEd\phi d\theta \quad \left(cm^3\cdot s^{-1}\right)$<br>$where \; \frac{\partial\Gamma(E)}{\partial E\partial\phi\partial\theta} = \frac{2E^2}{h^3c^2}\left(exp\left(\frac{E}{kT_{300K}}\right)-1\right)^{-1} \quad \left(cm^2\cdot s\cdot eV\cdot sr\right)^{-1}$<br>$B \approx 1\times10^{-10}cm^3/s$ |
| Transmission coefficient for recombination photons internal to diode (forward direction) [19,20] | $T_{back}^{forward}(\theta,E) = \frac{(1-R_{back})R_{front}\,exp\left[\frac{-(z+W)\alpha}{\cos\theta}\right]}{\left(1-R_{front}R_{back}\,exp\left[\frac{-2\alpha W}{\cos\theta}\right]\right)}$<br>$T_{front}^{forward}(\theta,E) = (1-R_{front})exp\left[\frac{-z\alpha}{\cos\theta}\right]\frac{R_{front}R_{back}\,exp\left[\frac{-2\alpha W}{\cos\theta}\right]}{\left(1-R_{front}R_{back}\,exp\left[\frac{-2\alpha W}{\cos\theta}\right]\right)}$ |
| Photon recycling factor [19,20] | $\varphi^{-1} = \frac{\sum_i^{Surfaces}\int_{z=0}^{z=W}\int_{\theta=0}^{\pi/2}\int_{\phi=0}^{\phi=2\pi}\int_{E=0}^{E=\infty} n^2\alpha(E)\frac{\partial\Gamma(E)}{\partial E\partial\phi\partial\theta}T_i(\theta,E)\sin\theta dEd\phi d\theta dz}{\int_{z=0}^{z=W}\int_{\theta=0}^{\theta=\pi}\int_{\phi=0}^{\phi=2\pi}\int_{E=0}^{E=\infty} n^2\alpha(E)\frac{\partial\Gamma(E)}{\partial E\partial\phi\partial\theta}\sin\theta dEd\phi d\theta dz} \quad \left(cm^3\cdot s^{-1}\right)$<br>integrate the term in the numerator for both front and back surfaces and for photons originating in both the forward and reverse directions<br>Ideal BSR: $\varphi_{BSR=100\%} \approx 40$ , Zero reflection at back : $\varphi_{AbsorbingSubstrate} \approx 4$ |
| Auger coefficient | $C_n = C_p = 2\times10^{-28}cm^6/s$ unless otherwise indicated |
| SRH Lifetime | Measured values give $\tau_{SRH}$ = 0.1 to 1μs for electrons. Intrinsic limit requires >>1μs |
| SRV | $S_n$=$S_p$ varied from 10cm/s to 2000cm/s [14,15] |
| Electron and hole mobility model [29] | $\mu_e = 420\frac{cm^2}{V\cdot s} + \frac{8500}{1+\left(\frac{N_D}{5\times10^{17}cm^{-3}}\right)^{0.7}}$ $\mu_h = 110\frac{cm^2}{V\cdot s} + \frac{500}{1+\left(\frac{N_A}{9\times10^{17}cm^{-3}}\right)^{0.66}}$ |
| Free carrier absorption in active region | Assumed to be negligible |

## References


[1] P.F. Baldasaro, J.E. Raynolds, G.W. Charache, D.M. Depoy, C.T. Ballinger, T. Donovan, and J.M. Borrego, "Thermodynamic analysis of thermophotovoltaic efficiency and power density tradeoffs," *J. Appl. Phys*., vol. 89, pp. 3319-3327, 2001.

[2] Timothy J. Coutts and James S. Ward, "Thermophotovoltaic and photovoltaic conversion at high-flux densities," *IEEE Trans. Electron Devices*, vol. 46, pp. 2145-2153, 1999.

[3] EJ Brown, PF Baldasaro, SR Burger, LR Danielson, DM Depoy, JM Dolatowski, PM Fourspring, GJ Nichols, WF Topper "The Status of Thermophotovoltaic Energy Conversion Technology at Lockheed Martin Corporation," in *Collect.. Tech. Pap. Int. International Energy Conversion Engineering Conference*, vol. 2, American Institute of Aeronautics and Astronautics Inc., 2004, pp. 1296-1315.

[4] B. Wernsman, R.R. Siergiej, S.D. Link, R.G. Mahorter, M.N. Palmisiano, R.J. Wehrer, R.W. Shultz, R.L. Messham, S. Murray, C.S. Murray, F. Newman, D. Taylor, D. Depoy, and T. Rahmlow, "Greater than 20% radiant heat conversion efficiency of a thermophotovoltaic radiator/module system using reflective spectral control," *IEEE Trans. Electron Devices*, vol. 51, pp. 512-516, 2004.

[5] T.D. Rahmlow, J.E. Lazo-Wasem, E.J. Gratrix, P.M. Fourspring, and D.M. Depoy "Design Considerations and Fabrication Results for Front Surface TPV Spectral Control Filters", in *Proc. Sixth Conference on Thermophotovoltaic Generation of Electricity*, vol. 738, AIP Conf. Proc., pp. 180-188, 2004.

[6] Patrick M. Fourspring and David M. DePoy, Thomas D. Rahmlow, Jr., Jeanne E. Lazo-Wasem, and Edward J. Gratrix, "Optical Coatings for Thermophotovoltaic Spectral Control," in Optical Interference Coatings on CD-ROM (The Optical Society of America, Washington, DC, 2004), ThE10.

[7] G.W. Charache, P.F. Baldasaro, L.R. Danielson, D.M. Depoy, M.J. Freeman, C.A. Wang, H.K. Choi, D.Z. Garbuzov, R.U. Martinelli, V. Khalfin, S. Saroop, J.M. Borego, "InGaAsSb thermophotovoltaic diode: Physics Evaluation", J. *Appl. Phys*., vol. 85, pp. 2247-2252, 1999.

[8] C.W. Hitchcock, R.J. Gutmann, J.M. Borego, I.B. Bhat, G.W. Carache, "Antimonide-based devices for thermophotovoltaic applications" , *IEEE Trans. Electron Devices*, vol. 46, pp. 2154-2161 1999.

[9] C.A. Wang, H.K. Choi, S.L Ransom, G.W. Charache, L.R. Danielson, and D.M. Depoy, "High-quantum-efficiency GaInAsSb/GaSb thermophotovoltaic devices", *Appl. Phys. Lett*., vol. 75, pp. 1305-1307, 1999.

[10] H.K. Choi, C.A. Wang, G.W. Turner, M.J. Manfra, D.L. Spears, G.W. Charache, L.R. Danielson, and D.M Depoy, " High performance GaInAsSb thermophotovoltaic devices with an AlGaAsSb window", *Appl. Phys. Lett*., vol. 71, pp. 3758-3760, 1997.

[11] M.W. Dashiell, J.F. Beausang, G. Nichols, D.M. Depoy, L.R. Danielson, H. Ehsani, K.D. Rahner, J. Azarkevich, P. Talamo, E. Brown, S. Burger, P. Fourspring, W. Topper, P.F. Baldasaro, C.A. Wang, R. Huang, M. Connors, G. Turner, Z. Shellenbarger, G. Taylor, Jizhong Li, R. Martinelli, D. Donetski, S. Anikeev, G. Belenky and S. Luryi, D.R. Taylor, J. Hazel "0.52 eV Quaternary InGaAsSb Thermophotovoltaic Diode Technology" in *Proc. Sixth Conference on Thermophotovoltaic Generation of Electricity*, vol. 738, pp. 404-414, AIP Conf. Proc., 2004.

[12]. S.M. Sze, *Physics of Semiconductor Devices, 2nd Edition*, John Wiley and Sons, Inc. 1981.

[13] W. Shockley and H.A. Queisser, "Detailed balance limit of efficiency of p-n junction solar cells", *J. Appl. Phys*., vol. 32, pp. 510-519, 1961.

[14] C. H. Henry, "Limiting efficiencies of ideal single and multiple energy gap terrestrial solar cells", *J. Appl. Phys*., vol. 51, pp. 4494-4500, 1980.

[15] S. Anikeev, D. Donetski, G. Belenki, S. Luryi, C.A. Wang, J.M. Borrego, G. Nichols, "Measurement of the Auger Recombination rate in p-type 0.54eV GaInAsSb by time-resolved photoluminescence", *Appl. Phys. Lett*., vol. 83, pp. 3317-3319, 2003.

[16] D. Donetski, , S. Anikeev, G. Belenky, S. Luryi, C.A. Wang, G. Nichols, " Reduction of interfacial recombination in GaInAsSb/GaSb double heterostructures", *Appl. Phys. Lett*., vol. 81, pp. 4769-4771, 2002.

[17] D. Donetski, S. Anikeev, N. Gu, G. Belenky, S. Luryi, C.A. Wang, D.A. Shiau, M. Dashiell, J. Beausang, and G. Nichols, "Analysis of recombination processes in 0.5-0.6eV epitaxial GaInAsSb lattice matched to GaSb", in *Proc. Sixth Conference on Thermophotovoltaic Generation of Electricity*, vol. 738, pp. 320-328, AIP Conf. Proc., 2004.

[18] W. van Roosbroeke and W. Shockley, "Photon-radiative recombination of electrons and holes in germanium", *Physical Review*, vol. 94, pp. 1558-1560, 1954.

[19] P. Asbeck, "Self-absorption effects on the radiative lifetime in GaAs-GaAlAs double heterostructures", *J. Appl. Phys*., vol. 48, pp. 820-822, 1977.

[20] A. Marti, J.L. Balenzategui, R.F. Reyna, "Photon recycling and Schockley's diode equation", *J. Appl. Phys*., vol. 82, pp. 4067-4075 1997.

[21] Martin A. Green, "Limits on the open-circuit voltage and efficiency of silicon solar cells imposed by intrinsic Auger processes", *IEEE Transactions on Electron Devices*, vol. ED-31, pp. 671-678, 1984

[22] R.K. Huang, C.A. Huang, M.K. Connors, G.W. Turner, "Hybrid Back Surface Reflector GaInAsSb Thermophotovoltaic Devices", in *Proc. Sixth Conference on Thermophotovoltaic Generation of Electricity*, vol. 738, pp. 329-336, AIP Conf. Proc.., 2004.

[23] R. Huang, C.A. Wang, C.T. Harris, M.K. Connors, D.A. Shiau "Ohmic Contacts to n-type GaSb and n-type GaInAsSb", *J. Electronic Materials*, vol. 33, pp 1406-1410, 2004.

[24] S.J. Adachi, "Optical Dispersion Relations for GaP, GaAs, GaSb, InP, InAs, InSb, AlGaAs, and InGaAsP" *J. Appl. Phys*., vol. 66, pp. 6030-6040, 1989.

[25] J.M. Olsen, R.K. Ahrenkiel, D.J. Dunlavy, B. Keyes, and A.E. Kibbler, "Ultralow recombination velocity at GaInP/GaAs Heterointerfaces" *Appl. Phys, Lett*., vol. 55, pp. 1208-1210, 1989.

[26] L.W. Molenkamp, G.L.M. Kampschoer, W. deLange, J.W.F.M Maes, and P.J. Roksnoer, "Ultralong minority-carrier lifetimes in GaAs grown by low-pressure organometallic vapor-phase epitaxy", *Appl. Phys. Lett*., vol. 54, pp. 1992-1994, 1989.

[27]A.G. Milnes and A.Y. Polyakov, "Review:Gallium Antimonide Device Related Properties", *Solid-State-Electronics*, vol. 36, pp. 803-818, 1993.

[28] C.K. Gethers, C.T. Ballinger, and D.M DePoy, in *Proc. Fourth Conference on Thermophotovoltaic Generation of Electricity*, vol. 460, pp. 335-348, AIP Conf. Proc., 1998.

[29] Expressions fit from mobility data of InGaAsSb layers grown on insulating GaAs substrates given in C.A. Wang, H.K. Choi, D.C. Oakley, G.W. Charache, *J. Crystal Growth*, vol. 195, p. 346, 1998.

**List of Figures**

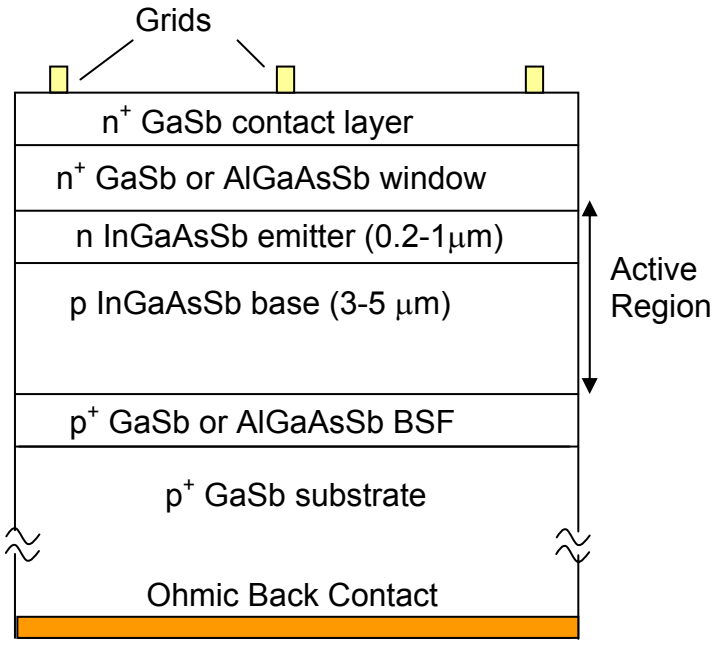


*0.53eV n/p InGaAsSb TPV*

Figure 1

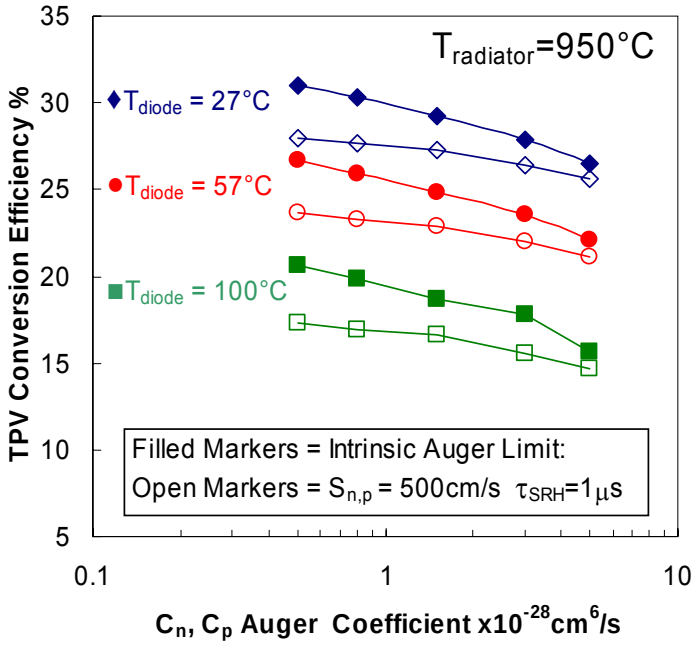
35
30
25
20
15
10
5
TPV Conversion Efficiency %
$T_{radiator}$=950°C
$T_{diode}$ = 27°C
$T_{diode}$ = 57°C
$T_{diode}$ = 100°C
Filled Markers = Intrinsic Auger Limit:
Open Markers = $S_{n,p}$ = 500cm/s $\tau_{SRH}$=1μs
0.1
1
10
$C_n$, $C_p$ Auger Coefficient x$10^{-28}$cm$^6$/s

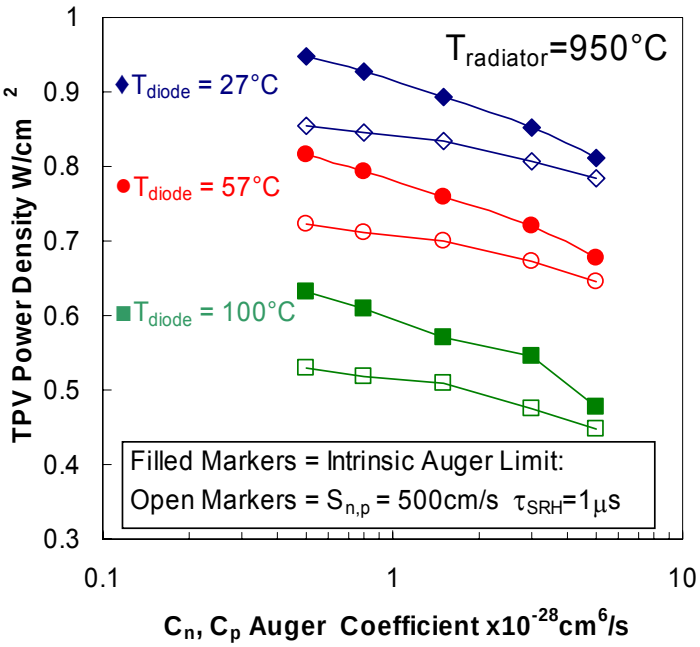
1
0.9
0.8
0.7
0.6
0.5
0.4
0.3
TPV Power Density W/cm$^2$
$T_{radiator}$=950°C
$T_{diode}$ = 27°C
$T_{diode}$ = 57°C
$T_{diode}$ = 100°C
Filled Markers = Intrinsic Auger Limit:
Open Markers = $S_{n,p}$ = 500cm/s $\tau_{SRH}$=1μs
0.1
1
10
$C_n$, $C_p$ Auger Coefficient x$10^{-28}$cm$^6$/s

Figure 2

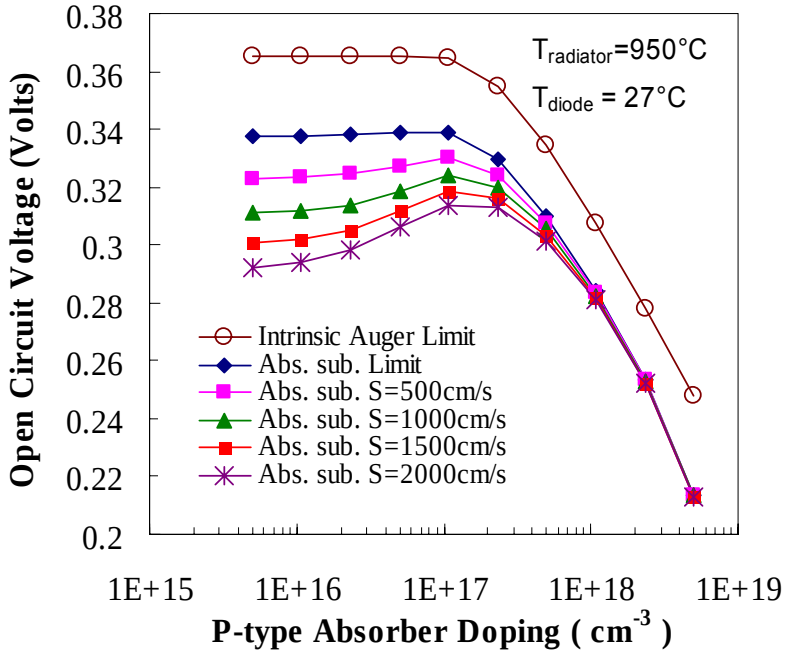


Figure 3

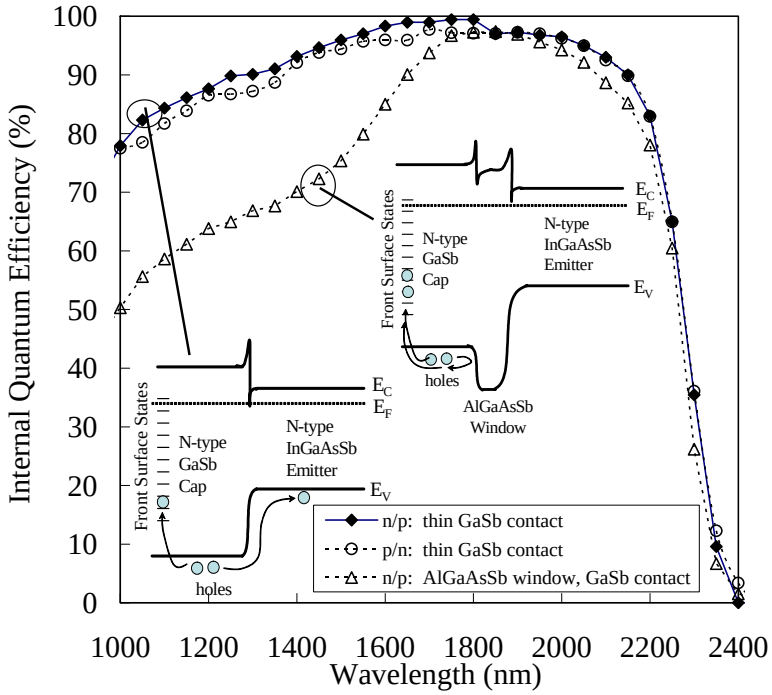


Figure 4.

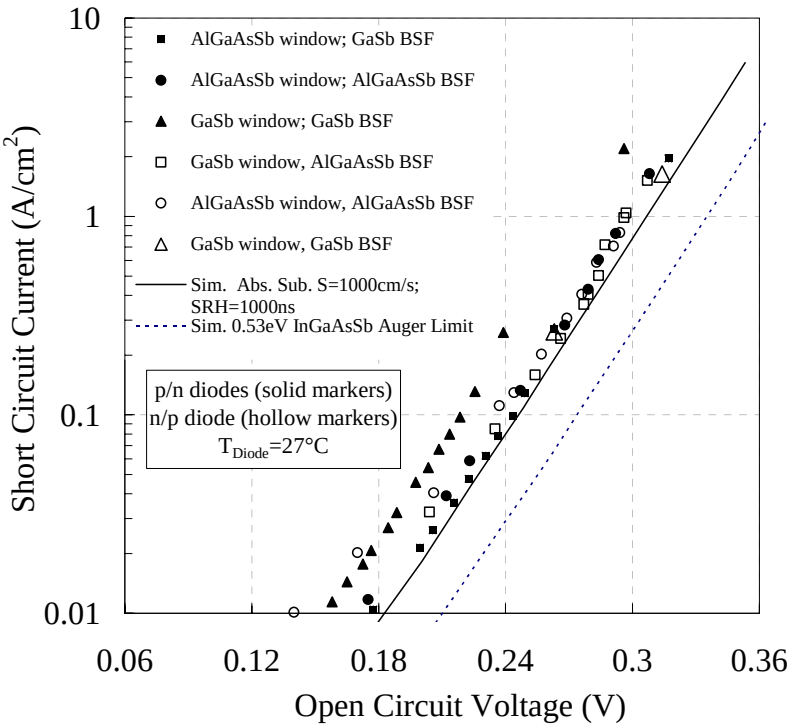


Figure 5

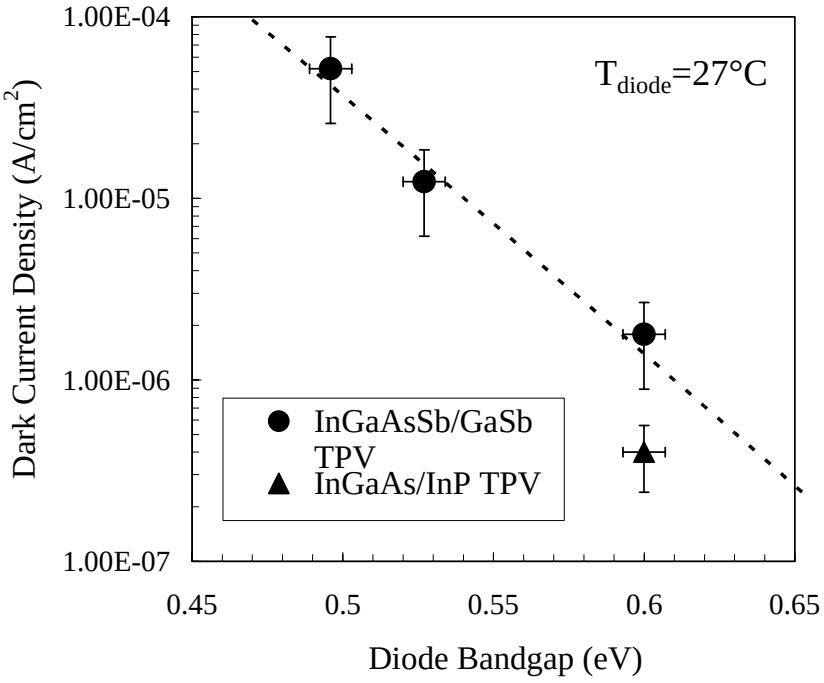


Figure 6